

Possible detection of two giant extrasolar planets orbiting the eclipsing polar UZ Fornacis[★]

Stephen B. Potter^{1†}, Encarni Romero–Colmenero¹, Gavin Ramsay^{2,6},
 Steven Crawford¹, Amanda Gulbis¹, Sudhanshu Barway¹, Ewald Zietsman^{1,4},
 Marissa Kotze^{1,5}, David A. H. Buckley¹, Darragh O’Donoghue¹,
 O. H. W. Siegmund³, J. McPhate³, B. Y. Welsh³ and John Vallergera³

¹South African Astronomical Observatory, PO Box 9, Observatory 7935, Cape Town, South Africa

²Armagh Observatory, College Hill, Armagh BT61 9DG

³Experimental Astrophysics Group, Space Sciences Laboratory, University of California Berkeley, CA 94720, USA

⁴Department of Mathematical Sciences, The University of South Africa, PO Box 392, UNISA, 0003, South Africa

⁵Astronomy Department, Astrophysics, Cosmology and Gravity Centre (ACGC), University of Cape Town, Rondebosch 7701, South Africa

⁶Mullard Space Science Laboratory, University College London, Holmbury St Mary, Dorking, Surrey RH5 6NT, UK

ABSTRACT

We present new high-speed, multi-observatory, multi-instrument photometry of the eclipsing polar UZ For in order to measure precise mid-eclipse times with the aim of detecting any orbital period variations. When combined with published eclipse times and archival data spanning ~ 27 years, we detect departures from a linear and quadratic trend of ~ 60 s. The departures are strongly suggestive of two cyclic variations of 16(3) and 5.25(25) years. The two favoured mechanisms to drive the periodicities are either two giant extrasolar planets as companions to the binary (with minimum masses of $6.3(1.5)M_{Jup}$ and $7.7(1.2)M_{Jup}$) or a magnetic cycle mechanism (e.g. Applegate’s mechanism) of the secondary star. Applegate’s mechanism would require the entire radiant energy output of the secondary and would therefore seem to be the least likely of the two, barring any further refinements in the effect of magnetic fields (e.g. those of Lanza et al.). The two planet model can provide realistic solutions but it does not quite capture all of the eclipse times measurements. A highly eccentric orbit for the outer planet would fit the data nicely, but we find that such a solution would be unstable. It is also possible that the periodicities are driven by some combination of both mechanisms. Further observations of this system are encouraged.

Key words: accretion, accretion discs – methods: analytical – binaries: close – novae, cataclysmic variables – X-rays: stars, planetary systems.

1 INTRODUCTION

Approximately 20% of the known cataclysmic variables (CVs, see the catalogue of Ritter & Kolb 2003) are polars, where the primary white dwarf has a sufficiently strong magnetic field to lock the system into synchronous rotation with the red dwarf secondary and to prevent completely the formation of an accretion disc.

The material from the secondary overflowing the Roche

lobe initially falls towards the white dwarf following a ballistic trajectory until, at some distance from the white dwarf, the magnetic pressure overwhelms the ram pressure of the ballistic stream. From this point on the accretion flow is confined to follow the magnetic field lines of the white dwarf. The now supersonic accreting material suddenly becomes sub-sonic at a shock region, which forms at some height above the white dwarf surface. The shock-heated material reaches temperatures of $\sim 10 - 50$ keV and is therefore ionised. The hot plasma cools by X-ray cooling, in the form of bremsstrahlung radiation. With sufficiently strong magnetic fields we find also cyclotron cooling, in the form of optical/infrared cyclotron radiation (e.g. ST LMi: Imamura,

[★] Based on observations made with the Southern African Large Telescope (SALT)

[†] sbp@sao.ac.za

Steiman-Cameron & Wolff, 2000, and Campbell, Harrison, Mason, Howell & Schwope, 2008). See e.g. Warner (1995) for a review of CVs and Cropper (1990) and Patterson (1994) for reviews of magnetic CVs.

UZ For is one of 15 known eclipsing polars and was discovered with *EXOSAT* (EXO 033319-2554.2) as a serendipitous X-ray source (Giommi et al. 1987; Osborne et al. 1988). Extensive followup observations at multi-wavelengths established a ~ 126.5 -min orbital period, one or two accretion spots depending on accretion state, with magnetic fields of ~ 53 MG and ~ 48 MG and a white dwarf mass of $\sim 0.7M_{\odot}$ (Beuermann, Thomas & Schwope 1988; Berriman & Smith 1988; Ferrario et al. 1989; Bailey & Cropper 1991). The eclipses of the accretion spots in UZ For are particularly rapid at 1-3 s and can only be resolved with high speed photometry. Bailey & Cropper (1991) were able to resolve the eclipse of the white dwarf photosphere during a low state and Perryman et al. (2001) were able to resolve two accretion spots during a higher accretion state. These distinct rapid photometric transitions are ideal for making accurate timing measurements and therefore searching for any long term period variations in UZ For. Some of the above-mentioned authors have combined their observations with previous eclipse measurements in order to obtain accurate eclipse ephemerides. In general, significant residuals were seen in the O-Cs (Observed - Calculated) of the orbital period, but no overall trend had been detected (e.g. Perryman et al. 2001). More recently, Dai et al. (2010) claim the existence of a third body orbiting UZ For in order to explain the O-C. However, their singular new eclipse measurement and subsequent derived orbital parameters are grossly incompatible with all of our new observations spanning ~ 10 years.

Nevertheless, recent results of long term studies of some CV related objects are beginning to show trends. Parsons et al. (2010) presented high-speed ULTRACAM photometry of 8 post-common-envelope-binaries. They detect significant departures from linearity in some of these systems and suggest magnetic braking or a third body as possible mechanisms to drive the O-Cs. High precision eclipse measurements of the post-common envelope binary NN Ser (Beuermann et al. 2010a) shows strong evidence for two additional bodies superposed on the binary's linear ephemeris. Significant and complicated departures from a linear ephemeris have also been seen in the eclipsing polar HU Aqr (Schwarz et al. 2009). They find that neither a sinusoidal nor a quadratic ephemeris are sufficient to describe their O-C departures, thus more eclipse observations over the next few years will be needed in order to refine the ephemerides. Qian et al. (2010) discovered that the O-C curve of the eclipsing polar DP Leo shows a cyclic variation with a period of 23.8 years. They claim that this is as a result of a giant extrasolar planet orbiting DP Leo, recently refined by Beuermann et al (2010b).

Here we present new high-speed *HIPPO*, *BVIT*, *SALTICAM* and *UCTPOL* photometry of UZ For, spanning 10 years, and use these observations to determine accurate mid-eclipse times of the main accretion spot in UZ For. We combine these with previous mid-eclipse times, that we either measure from archival data or extract from the literature, and analyse for any period variations in UZ For. Note

that adding these newer data to timing from the literature gives a baseline of 27 years.

2 OBSERVATIONS

All of the eclipse times extracted from the literature were published as Heliocentric Julian Dates (HJD). We have assumed that the Coordinated Universal Time (UTC) system was used in all cases as this was not explicitly stated in any of the publications. We re-corrected all times for the light travel time to the barycenter of the solar system, converted to the barycentric dynamical time system (TDB) and the times are listed (table 1) as Barycentric Julian Date (BJD; see Eastman, Siverd & Gaudi 2010 for achieving accurate absolute times and time standards). By doing this we have removed any timing systematics, particularly due to the unpredictable accumulation of leap seconds with UTC, and effects due to the influence of primarily Jupiter and Saturn when heliocentric corrections only are applied. We either calculate or re-calculate appropriate errors depending on the S/N and time resolution at the time of the spot ingress and egress. Table 1 also lists the eclipse width of the accretion spot and the observatory/instrument used.

All of our new observations were also converted to BJD. We note that our new ground based instruments were synchronised to GPS to better than a milli-second. Given the high-speed nature of these instruments, their timing accuracies have been verified through simultaneous multi-instrument observations. The remaining space observatories have documented reports on the performance of their on-board clocks.

2.1 Eclipse times from the literature

The earliest UZ For eclipse measurements were made using *EXOSAT* and published by Osborne et al. (1998). The data are of poor time resolution but are at a sufficiently early epoch to provide constraints for model fitting. Beuermann et al. (1988) and Ferrario et al. (1989) observed multiple eclipses spectrophotometrically. These are also of very low time resolution, however the combination of multiple eclipses provides usable data. Allen et al. (1989) presented the first high speed photometry that could resolve the accretion spot. A typographical error in the eclipse time was corrected by Ramsay (1994). This was soon followed with more high quality optical low-state photometry by Bailey & Cropper (1991) and high-state photometry by Imamura & Steiman-Cameron (1998) and *EUVIE* light curves by Warren et al. (1995). An additional high quality STJ eclipse was also published by de Bruijne (2002) and three more, with the same instrument by Perryman et al. (2001). From the latter data we were able to obtain the raw observations and re-measure and confirm the eclipse times.

2.2 ROSAT (1991)

Observations were retrieved from the HEASARC archive and events were extracted using an aperture centered on the source and also a background region. The resulting light curves were subtracted after appropriate scaling from the

differing areas. The observations spanned ~ 1 day and multiple eclipses were covered. The reduced data were binned and folded on the orbital period in order to produce a single eclipse light curve from which the eclipse was measured.

2.3 HST FOS (1992)

UZ For was observed by HST with FOS on 11th June 1992 in two consecutive, RAPID mode observations consisting of 925 spectra each with 1.64s exposure times. This data set was originally published in Stockman & Schmidt (1996), but their mid-eclipse times were not quoted. Therefore the HST data products from this observation were downloaded from the HST archive at the MAST. The flux- and wavelength-calibrated individual spectra were extracted and the flux summed-up between 1255 and 1518Å (far UV) to create a lightcurve. The far UV part of the spectrum was chosen as this seems to have the least contribution from the accretion stream. The end-times for each spectra were obtained from the observation header keywords and the group-delay-time subtracted in order to obtain times of start of each exposure. Two consecutive eclipses were observed and folded and binned into a single eclipse from which measurements were made.

2.4 EUVE 1993 and 1995

UZ For was observed with EUVE on the 18th November 1993 and on the 15th Jan 1995 for 102ks and 76ks respectively. These data were retrieved from the STScI archive and reduced following the recipe from <http://archive.stsci.edu/euve/>. Lightcurves were produced using the `xray.xtiming` package in IRAF with a 1s time resolution. For each observation, multiple eclipses were covered which were folded and binned into two single eclipses from which measurements were made.

2.5 UCTPOL 2002 and 2005

One unfiltered and two BG39 filtered eclipses were obtained in 2002 with the University of Cape Town photo-polarimeter (UCTPOL) at 10 second time resolution. Two eclipse times were extracted: one from the unfiltered and the second from the folded BG39 filtered eclipses. Three unfiltered eclipses were obtained in 2005 at 10 and 1 second time resolution. Two eclipse times were extracted. On both occasions, simultaneous linear and circular polarimetric observations were also made and reduced as in Cropper (1985).

2.6 XMMOM 2002

Observations were made in fast-mode using the *XMM-Newton* Optical Monitor (Mason et al 2001) between Aug 7 and Aug 8 2002; two orbits after UCTPOL observations. The UVW1 filter was used (center wavelength 2910 Å, FWHM 500 Å) and the data were reduced using `omfchain` running under SAS v9.0. Although three consecutive eclipses were observed, two had incomplete coverage. Nevertheless, upon folding and binning, a high signal-to-noise eclipse profile was obtained and eclipse measurements taken.

2.7 SWIFT 2005

Observations were made in event mode using the *SWIFT* UV Optical Telescope (Roming et al 2005) between Feb 2 and Feb 6 2005. There were a number pointings, some lasting a few 100 sec and others a few 1000 sec. The *U* filter (center wavelength 3450 Å, FWHM 875 Å) and the *V* filter were used. Light curves were extracted using apertures centered on the source (radius 3'') and also a source free background region with much larger aperture radius. The light curve was generated by suitably scaling the size of the apertures. Two eclipses were observed in full, one of which was simultaneous with the UCTPOL observations.

2.8 SALTICAM 2007

UZ For was observed with SALTICAM (O'Donoghue et al. 2006) on SALT on 12 November 2007. SALTICAM was in slot-mode configuration, allowing a time resolution of 1s with no deadtime. The data were reduced using the SALT slottools data reduction package (Crawford et al. 2010). One eclipse of high time resolution and signal to noise was observed from which measurements were made.

2.9 BVIT 2009

BVIT (Berkeley Visible Imaging Tube: Siegmund et al. 2008) is a visible photon counting detector designed as a guest facility on the SALT to provide very high time resolution (< 25 nanoseconds) and high signal to noise, full imaging photometry. UZ For was observed during a BVIT commissioning run on 25th January 2009 simultaneous with the HIPPO on the 1.9m telescope of the South African Astronomical Observatory. The data were extracted making use of the IDL data reduction software developed by the instrument team and binned into 0.5s bins. One eclipse of high time resolution and s/n was observed from which measurements were made.

2.10 HIPPO January 2009, September 2010, October 2010 and November 2010

Unfiltered photo-polarimetric observations were made with the HIPPO (HI speed Photo-Polarimeter: Potter et al. 2010) on four separate occasions and reduced as in Potter et al. (2010). The single eclipse in January 2009 was observed simultaneously with the BVIT observations. Multiple eclipses were observed on the other occasions which were folded and binned from which measurements were made.

3 RESULTS

3.1 The eclipses

A sample of our new and archival eclipse data is shown in Fig 1 phased on our new ephemeris (see below and table 2). The eclipse profiles are of varying quality and at multiple wavelengths. All of the eclipses can be understood in the framework of the standard polar model and from the general literature on UZ For (see section 1). UZ For undergoes

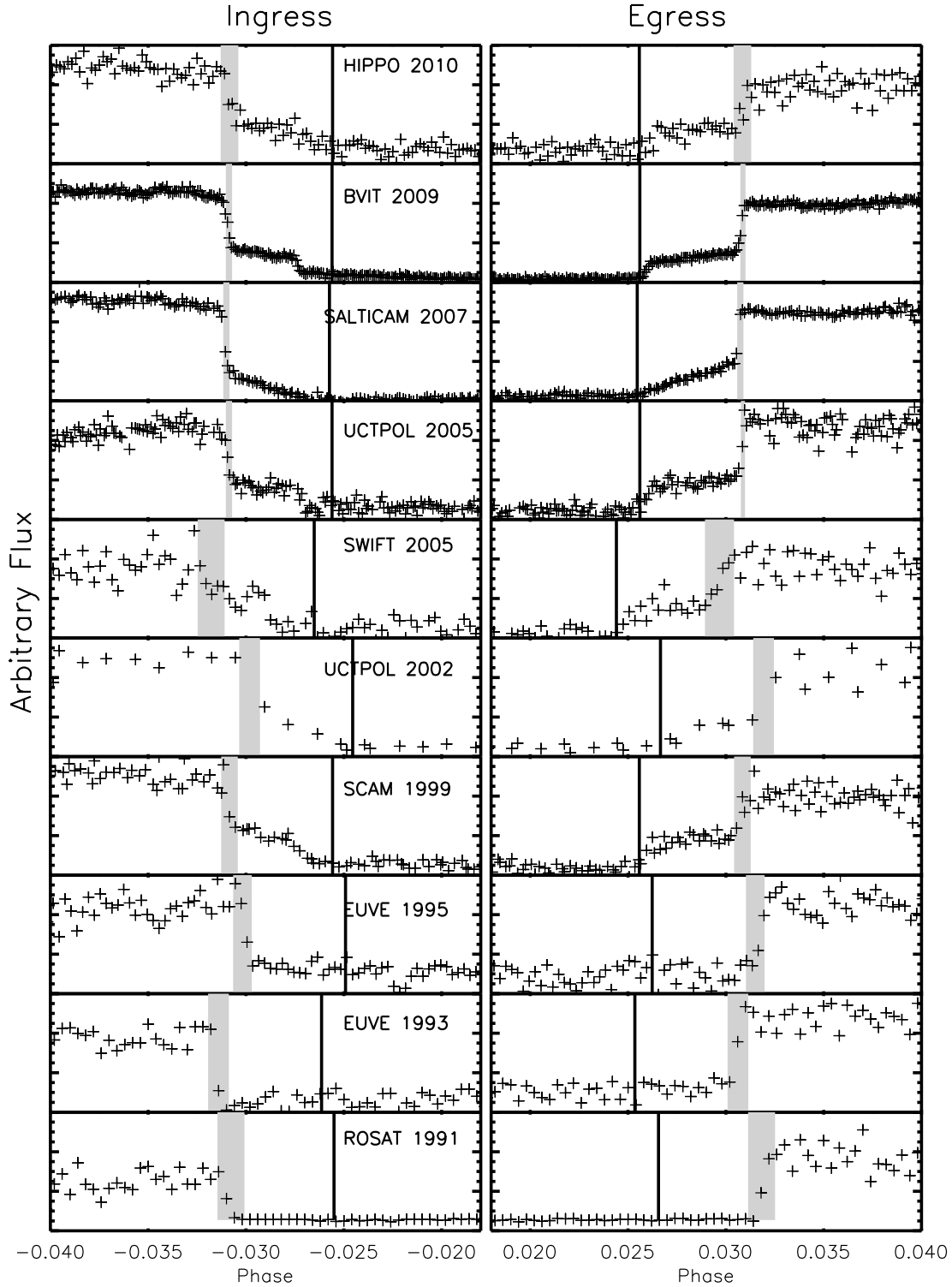


Figure 1. A sample of our new eclipse observations phased on our new ephemeris (section 4.2) Vertical grey bars indicate ingress and egress of the main accretion spot. Solid vertical bars indicate times of white dwarf ingress and egress assuming a duration of 40s.

periods of either one (e.g. Bailey & Cropper 1991) or two-pole (e.g. Perryman et al. 2001) accretion states, which has been most clearly captured by our SALTICAM (2007) and BVIT (2009) observations respectively. During both accretion states the rapid fall and rise in flux at phases ~ -0.031

and ~ 0.031 correspond to the ingress and egress of the main accretion region. During the two-pole accretion state a second accretion region is additionally present, seen as the fall and rise in flux at phases ~ -0.027 and ~ 0.027 . The remaining gradual fall and rise during phases ~ -0.031 to -0.025

Table 1. Mid-eclipse times of the main accretion spot of UZ For. BJD_{TDB} is the Barycentric Julian Date in the barycentric dynamical time system. Times have also been barycentrically corrected. ¹de Bruijne et al. (2002), ²Perryman et al. (2001), ³Imamura & Steiman-Cameron (1998), ⁴Warren et al. (1995), ⁵Ramsay (1994), ⁶Bailey & Cropper (1991), ⁷Allen et al. (1989), ⁸Ferrario (1989), ⁹Beuermann et al. (1988), ¹⁰Osborne et al. (1988).

Cycle	$\text{BJD}_{TDB}+2400000$	ΔBJD_{TDB}	Width(sec)	Observatory/Instrument
23913	55506.42703435	0.00001	468(2)	1.9m/HIPPO
23595	55478.48583116	0.00001	468(2)	1.9m/HIPPO
23277	55450.54462082	0.00001	467(2)	1.9m/HIPPO
16526	54857.36480850	0.00001	469(2)	1.9m/HIPPO
16526	54857.36480517	0.0000086	469(1)	SALT/BVIT
11518	54417.33472170	0.0000086	468(1)	SALT/SALTICAM
34	53408.28808581	0.0000086	469(1)	1.9m/UCTPOL
23	53407.32157438	0.00001	469(2)	1.9m/UCTPOL
0	53405.30066303	0.000035	469(3)	1.9m/UCTPOL
-11.0	53404.33404192	0.00006	467(4)	SWIFT
-10362	52494.83919610	0.000087	479(8)	XMM OM
-10365	52494.57562568	0.000035	469(3)	1.9m/UCTPOL
-10376	52493.60905802	0.00007	469(6)	1.9m/UCTPOL
-18023	51821.70239393	0.00001	467(2)	WHT/SCAM 2000 ¹
-21360	51528.49543399	0.00002	468(2)	WHT/SCAM 1999 ²
-21361	51528.40757990	0.00002	468(2)	WHT/SCAM 1999 ²
-21429	51522.43272958	0.00002	468(2)	WHT/SCAM 1999 ²
-38508	50021.779388	0.00005		CTIO 1m/Photometer ³
-38543	50018.704108	0.00005		CTIO 1m/Photometer ³
-41537	49755.634978	0.00005		CTIO 1m/Photometer ³
-41538	49755.547148	0.00005		CTIO 1m/Photometer ³
-41560	49753.614028	0.00005		CTIO 1m/Photometer ³
-41571	49752.647568	0.00005		CTIO 1m/Photometer ³
-41790	49733.40501704	0.00004	467(4)	EUVE
-46605	49310.33259382	0.00003	471(4)	EUVE
-46988	49276.680055	0.00004		EUVE ⁴
-52587	48784.72141928	0.00003	463(4)	HST
-56024	48482.72808573	0.0001	477(5)	ROSAT ⁵
-63462	47829.18486375	0.00003		AAT ⁶
-63474	47828.130520	0.00003		AAT ⁶
-63476	47827.954780	0.00003		AAT ⁶
-67915	47437.919920	0.00003	466.5(2.5)	2.3m Steward Obs. ^{7,5}
-71248	47145.064339	0.0002		AAT ⁸
-71451	47127.227739	0.0002		AAT ⁸
-71452	47127.139439	0.0002		AAT ⁸
-71786	47097.792559	0.0002		ESO/MPI 2.2m ⁹
-71821	47094.717359	0.0002		ESO/MPI 2.2m ⁹
-71857	47091.554239	0.0002		ESO/MPI 2.2m ⁹
-71868	47090.587789	0.0002		ESO/MPI 2.2m ⁹
-71889	47088.742549	0.0002		ESO/MPI 2.2m ⁹
-79193	46446.973809	0.00016		EXOSAT ¹⁰
-89206	45567.177597	0.00016		EXOSAT ¹⁰

and ~ 0.025 to 0.031 is attributed to the ingress and egress respectively of the white dwarf photosphere and takes about 40s each.

3.2 The O-C

In table 1 we list all of our new mid-eclipse times as well as those we have measured from archival data or extracted from the literature. The orbital period calculation of Perryman et al. (2001) was used to calculate the cycle number for each eclipse. The period is sufficiently accurate to unambiguously assign cycle counts to the entire ~ 27 years of eclipses. The eclipse observed in our 2005 UCTPOL photometry was used

to define the epoch (cycle 0). This period and epoch were next used as the starting point to perform a least-square quadratic fit with appropriate weighting set by the eclipse error measurements. The resulting fit gives a reduced $\chi^2 > 95$ with peak-to-peak residuals of $\sim 60 - 80$ s. Note that we have not included the eclipses of Dai et al. (2010) in our analysis as their O-Cs are over 300s compared to our quadratic ephemeris. We believe either their measurement and/or time standard conversion to be in error.

It is immediately apparent that there are significant departures from the quadratic ephemeris with a trend that appears to be periodic (see top plot of fig 2 for residuals, albeit from a different quadratic fit: see below).

Table 2. Mid-eclipse ephemerides of the main accretion spot of UZ For and corresponding planet model parameters. Ephemeris parameters correspond to the *representative* solution (Fig 3) and are rounded off to the 1 sigma errors. The planet parameter errors were calculated using the range in parameter space of possible solutions and not the smaller 1 sigma errors of any one fit. Minimum planet masses are listed assuming coplanarity. $M_{3,4,fn c}$ is the mass function. The combined mass of the primary and secondary stars are assumed to be $0.84M_{\odot}$.

Quadratic term:	$T_0 = 2453405.30086(3)$ d $P_{bin} = 0.087865425(2)$ d $A = -7(2)10^{-14}$	Planet Parameters:
1st Elliptical term:	$v_3 = (E+T_3)f_3$ $T_3 = 60383(416)$ (binary cycle) $f_3 = 0.000098(3)$ (cycles/binary cycle) $\varpi_3 = 0.85(5)$ $K_{bin,(3)} = 0.00025(2)$ d $e = 0.04(5)$	$M_{3,fn c} = 2.9(1.1)10^{-7}M_{\odot}$ $M_{3,Jup} = 6.3(1.5)$ $P_3 = 16(3)$ years $a_3 = 5.9(1.4)$ AU $a_{1,2} = 0.042(1)$ AU
2nd Elliptical term:	$v_4 = (E+T_4)f_4$ $T_4 = 4833(215)$ (binary cycle) $f_4 = 0.000288(2)$ (cycles/binary cycle) $\varpi_4 = 1.20(6)$ $K_{bin,(4)} = 0.000141(6)$ d $e = 0.05(5)$	$M_{4,fn c} = 5.3(5) 10^{-7}M_{\odot}$ $M_{4,Jup} = 7.7(1.2)$ $P_4 = 5.25(25)$ years $a_4 = 2.8(5)$ AU $a_{1,2} = 0.025(1)$ AU

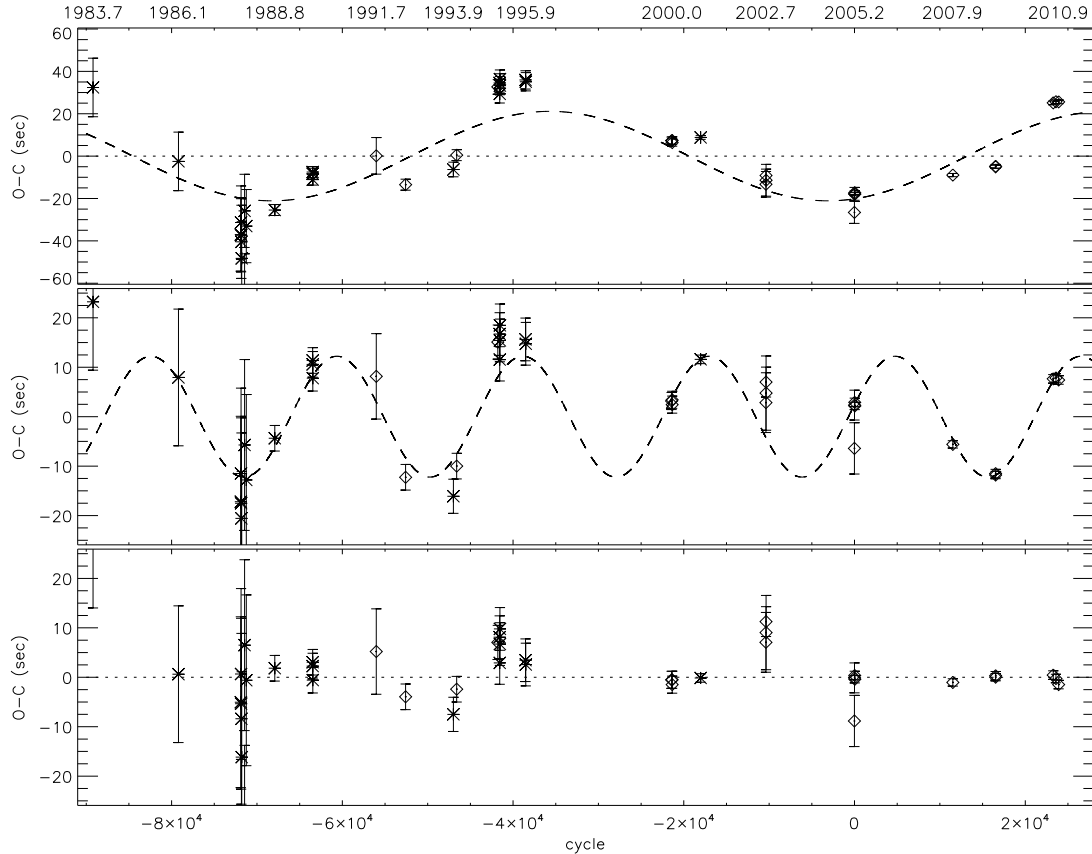


Figure 2. The O-C after successive subtraction of the three terms comprising our new eclipse ephemeris. Top: O-C after subtraction of the quadratic term with the first elliptical term overplotted (dashed curve). Middle: O-C after subtraction of the first elliptical term overplotted (dashed curve). Bottom: The final O-C residuals after subtraction of the second elliptical term. Diamonds are our new data or data that we have reduced from archives. Crosses are eclipse times from the literature and converted (by us) to BJD_{TDB} .

We next investigated the solutions resulting from models consisting of a quadratic plus an elliptical fit to the eclipse times. A best reduced χ^2 of 6.2 was achieved. An F-test shows that it is the better model (compared to the quadratic ephemeris) with a confidence of $> 99.999\%$ even though the elliptical term adds 5 more parameters to the model.

However significant residuals still remain, (~ 10 s) for some of the eclipse times (not shown). We next attempted a simultaneous quadratic plus two ellipticals fit to the eclipse times. The second elliptical term adds a further five parameters to the model, giving 13 in total. Therefore, given the large number of parameters, a grid of starting parameters for minimisation was required in order to explore the resulting degeneracy in the solutions. Approximately 10^7 minimisations were calculated. During minimisation all 13 parameters were free to vary. Predictably, the results have better reduced χ^2 but with degeneracy in many of the parameters. Formally the F-test confirms that adding a second elliptical term is the better model with a high level of confidence ($> 99.9999\%$) for the solutions with reduced $\chi^2 = 1.0$. Other solutions with reduced $\chi^2 = 4.0$ and 3.0 are also significantly better with a 98% and 99.9995% confidence respectively. We explore the degeneracy in the multi-dimensional χ^2 space in section 4.2.

4 DISCUSSION

4.1 The O-C

Our results suggest that the deviations in the eclipse O-C are best described by the combination of a quadratic term plus two elliptical terms. This is highly suggestive of both secular and cyclic period variations.

Period changes in binary systems are generally understood to be due to gravitational radiation, magnetic braking, solar-type magnetic cycles in the secondary star (Applegate's mechanism) and/or the presence of a third body in an orbit around the binary.

Applegate's mechanism and/or the presence of a third body would be more consistent with cyclic variability. The latter would produce strictly periodic cycles while non-strictly periodic cycles would be expected from the former mechanism. Therefore, we next look at each of these mechanisms in turn.

4.2 Tertiary and quaternary components

We now explore the degeneracy in the multi-dimensional χ^2 space of the model fits containing one quadratic plus two elliptical terms in the context that the variations are due to the effect of third and fourth bodies in the system. Then the changes in the O-C arise because of the light-time effect caused by the gravitational influence of the additional bodies.

As a first step, we plot the distribution of the period of the two elliptical orbits for those solutions which had reduced $\chi^2 < 2.5$ (Fig 3). The starting grid, for minimisation, had period values between 2 and 50 years and Fig 3 shows that the minimised solutions have clustered in the period ranges $\sim 13 - 19$ and $\sim 5 - 5.5$ years.

All of the solutions with reduced $\chi^2 \leq 1.0$ ($\chi^2 \leq 28$,

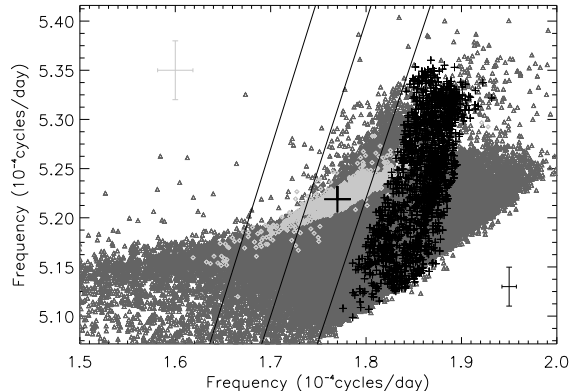


Figure 3. The reduced χ^2 parameter space for the two elliptical periods. Black crosses, dark grey triangles and light grey diamonds are the solutions with reduced $\chi^2 < 1.0$, $1.0 < \chi^2 < 2.5$ and $1.0 < \chi^2 < 2.5$ respectively. The diamonds have the additional constraint of both eccentricities < 0.1 . The large black cross represents the location of the solution shown in Fig 2 with parameters listed in table 2. From left to right, the diagonal lines represent contours of constant period ratios of 3.1, 3.0 and 2.9. Typical one sigma errors are shown in the top left and bottom right corners.

shown as the black crosses in Fig 3) show periods centered on approximately 5.3 and 15 years, giving a period ratio of $Rp \sim 2.8$. The corresponding predicted eccentricities of these solutions are $\gg 0.1$ for both ellipses. We performed N-body simulations on a sample of these solutions. The Euler method was used with sufficiently small time steps to ensure accurate calculations. We tested the accuracy of our code by first applying it to single elliptical orbits comparable to the innermost high eccentricity orbit. Our code preserves the eccentricity and the semi-major axis to better than 10%, and the periastron angle to < 0.1 radians over a time period corresponding to $> 10^5$ orbits of the outermost body. We then defined orbital solutions that have essentially the same two planet orbital elements to the starting conditions after $> 10^5$ orbits of the longer period as stable. As expected, we found that they all are very unstable orbits and are therefore unrealistic solutions.

We next looked at the solutions with reduced χ^2 in the range $1.0 < \chi^2 < 2.5$, which are shown as the dark grey triangles in Fig 3. They occupy a larger area of the plot which overlaps with the previous solutions. However most of these solutions still require the longer period elliptical to have a large eccentricity (> 0.1 and typically 0.4). N-body simulations within this parameter range also revealed unstable orbits.

We therefore identified those solutions which had orbital eccentricities < 0.1 for both planets and which had stable orbits according to our N-body simulations. These are represented as the light grey diamonds in Fig 3 which also overlap with the higher eccentric solutions presented above. However, the best of these solutions give $\chi^2=58$ (28 dof, giving $\chi^2_{\nu}=2.06$), which is a significantly poorer fit compared to our best-fit highly eccentric orbital solutions and also gives a formally poor fit to our data.

We note that our models assume the two planets to be

co-planar. There may yet be a set of realistic, more eccentric, solutions if the planets have inclined orbits with respect to each other. We have not investigated this additional parameter space as our data set is not of sufficient quality nor quantity to warrant it.

Given these caveats, in order to calculate the implied two planet parameters, we selected the best-fit low eccentric and stable solutions. Additionally we applied period errors that encompass the whole range of solutions in Fig 3. We note that the two planet parameters calculated below are not specific to this one best-fit solution but are representative of all the solutions with reduced $\chi^2 < 2.5$ shown in Fig 3. The calculations are independent of the eccentricities. This particular solution is marked as the large black cross in Fig 3, the two elliptical parameters are listed in table 2 and over-plotted on the O-C in Fig 2.

The amplitudes of the oscillations can be used to calculate the projected distances $asin(i)$ from the center of mass of the binary to the center of mass of each of the triple systems (0.042(1) and 0.025(1) AU for the long and short respectively). Setting the binary mass to be $0.7M_\odot + 0.14M_\odot$ gives the corresponding mass functions ($f(m_{3,4}) = 2.9 \times 10^{-7}M_\odot, 5.3 \times 10^{-7}M_\odot$). With the binary inclination at $i = 80^\circ$ the respective minimum masses for the third and fourth bodies (assuming they are in the plane of the binary) are $0.006(1) M_\odot$ and $0.007(1) M_\odot$ and would therefore qualify as extrasolar giant planets ($6.3(1.5)M_{Jup}$ and $7.7(1.2)M_{Jup}$) for orbital inclinations $i_3 > 25^\circ, i_4 > 32^\circ$ respectively. The quoted errors include the range in periods shown in Fig 3 and not the formal one sigma errors of one of the solutions. In addition, the quoted errors include the propagated uncertainties in the inclination and binary mass. These parameters are summarised in table 2.

The equation for the times (T) of mid-eclipse of the main accretion spot are then given by:

$$\begin{aligned} T(BJD_{TDB}) &= T_0 + P_{bin}E + AE^2 \\ &+ K_{bin,(3)} \sin(v_3 - \varpi_3) \frac{(1 - e_{(3)}^2)}{(1 + e_{(3)} \cos(v_3))} \\ &+ K_{bin,(4)} \sin(v_4 - \varpi_4) \frac{(1 - e_{(4)}^2)}{(1 + e_{(4)} \cos(v_4))} \end{aligned}$$

T_0, P_{bin}, A, E are the time of epoch, the binary orbital period (days), the quadratic parameter (related to the rate of period decrease by $\dot{P}_{bin} = 2A/P_{bin}$) and the binary cycle number which comprise the quadratic term of the ephemeris. In the context that the two elliptical terms are due to third and fourth bodies in the system, then the parameters of the elliptical terms are: $K_{bin,(3,4)}$ are the amplitudes of the eclipse time variations as a result of the light-travel-time effect of the two bodies, $v_{(3,4)}$ are the true anomalies of the two bodies, which progresses through 2π over the orbital periods ($P_{(3,4)}$) and are functions of E , the times of the periastron passages ($T_{(3,4)}$) and the orbital frequencies (in cycles per binary orbital cycle) of the two bodies ($f_{(3,4)}$). $e_{(3,4)}$ are the eccentricities and $\varpi_{(3,4)}$ are the longitudes of periastron passage measured from the ascending node in the plane of the sky. Similar elliptical variations have been seen in NN Ser and DP Leo (Beuermann et al 2010a,b).

Fig 2 shows the fit and the O-C residuals after successive

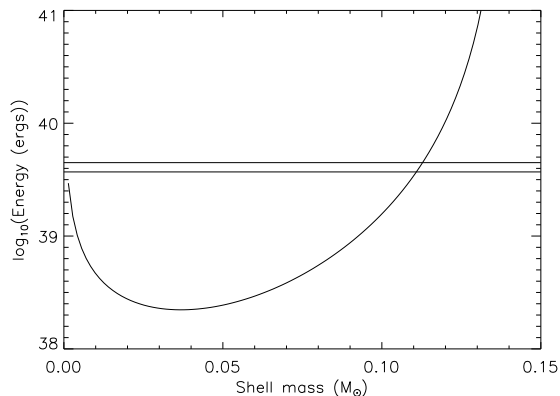


Figure 4. Solid curve shows the energy required to effect the period change observed in UZ For as a function of assumed shell mass, using Applegate’s (1992) mechanism. The two horizontal lines represent the total radiant energy of the secondary (assuming $2880 < T_{eff} < 3020K$) and hence the amount of energy available.

subtraction of the three terms comprising our new eclipse ephemeris with parameters listed in table 2. The top and middle plots show that the two elliptical terms describe the time of eclipse variations very well. The lower plot shows the final O-C residuals after subtraction of the full ephemeris. Some residuals still remain which could be reduced further if larger eccentricities were permitted, particularly for the outer planet. Such orbital solutions may exist, especially given the possible indication that the planets could be locked in a 3:1 ratio. However better sampled observations are required to further constrain the solutions.

4.3 The secular variability

The secular variability amounts to a decrease in the orbital period of $\dot{P}_{bin} = -1.56(5) 10^{-12} s s^{-1}$. Of the 1416 solutions that comprise the ‘chosen’ parameter space (light grey area in Fig 3) only one solution showed a \dot{P}_{bin} consistent with 0. It has a reduced $\chi^2 = 2.6$. The rest predict a minimum in the period decrease rate of $\dot{P}_{bin} = -1.0 10^{-12} s s^{-1}$. Formally an F-test shows that adding the quadratic parameter to the ephemeris is the better model with a 99.99% level of confidence ($\chi^2 = 109, 86$ for 30, 29 degrees of freedom for the two models respectively).

Similar levels of period decrease has been detected in other similar short period binaries e.g. DP Leo (Schwope et al. 2002), NN Ser (Brinkworth et al. 2006) and HU Aqr (Schwarz et al. 2009) for which gravitational radiation and magnetic braking have been shown to be either insufficient or problematic in the framework of the standard CV evolutionary model. Future observations are needed to show if these variations are indeed secular or periodic.

4.4 Applegate mechanism

Applegate (1992) proposed that solar-like magnetic cycles would drive shape changes in the secondary, thus redistributing the angular momentum within the star, changing its oblateness. This then leads to a change in its quadrupole

moment and consequently a change in orbital period at the expense of some energy. This has been the preferred mechanism to explain such cyclic variations in CVs and other long period close binaries (Algol, RS CVn and W UMa stars).

Following the prescription of Applegate (1992), the energy required to generate a period change is:

$$\Delta E = \Omega_{dr} \Delta J + \frac{\Delta J^2}{2I_{eff}}$$

The initial differential rotation $\Omega_{dr} \Delta J$ is set to zero in order to calculate the minimum energy required. The effective moment of inertia $I_{eff} = I_S I_* / (I_S + I_*)$ is calculated by assuming the star is separated into a shell I_S and a core I_* . We experimented with a range of shell masses. ΔJ is the change in angular momentum and is given by

$$\Delta J = \frac{-GM^2}{R} \left(\frac{a}{R} \right)^2 \frac{\Delta P}{6\pi}$$

We used the secondary star mass from Bailey & Cropper (1991) namely $M = 0.14M_\odot$ and the corresponding radius $R = 0.177R_\odot$ following Patterson (1984). $a = 5.5 \times 10^8 m$ is the binary separation using $a = 3.53 \times 10^{10} (M_1/M_\odot)^{1/3} (1+q)^{1/3} P_{orb}^{2/3} (h)$ (Warner 1995, equation 2.1b). ΔP can be obtained from equation (38) of Applegate (1992) relating the amplitude of orbital period modulation and the amplitude of the O-C oscillation:

$$\frac{\Delta P}{P} = 2\pi \frac{O-C}{P_{mod}}$$

where P and P_{mod} are the orbital and modulation period respectively (using P_3 listed in table 2). The solid curve in Fig. 4 shows the minimum energy required to drive the maximum observed period change in UZ For, as a function of assumed secondary shell mass. The two horizontal lines represent the total radiant energy of the secondary $L = 4\pi R^2 \sigma T^4$ over the modulation period, assuming $2880 < T_{eff} < 3020K$, which appears to be more than sufficient to drive the Applegate mechanism. The situation is not so clear cut if one instead integrates over shells and allows for the quadrupole moment of the core (using the calculations of Brinkworth et al. 2006). This raises the minimum energy by about an order of magnitude, which makes it comparable, at minimum, to the energy of the star.

We should add that Lanza et al. (1998) propose a prescription that is more energy efficient than the Applegate mechanism, perhaps by a factor of two. Therefore, with further refinements, magnetic fields may yet be shown to able to drive the period changes seen here.

4.5 Spot motion

The eclipse times are derived from the observed ingress and egress times of the accretion spot and not the center of the white dwarf itself. Therefore the observed O-Cs could be as a result of motion of the spot on the white dwarf. In addition, the egress and ingress of the white dwarf photosphere has been observed to take about 40 seconds (seen unambiguously in the low state observations of Bailey & Cropper (1991) and confirmed in our low state *SALTICAM 2007* observations) and therefore could accommodate a $\sim 40 - 60s$ of spot motion.

To assess this possibility we investigated the actual morphologies of the eclipse profiles in order to measure the relative phases of the white dwarf photosphere ingresses and egresses to that of the main accretion spot. Accordingly, we display a sample of our eclipse observations in Fig. 1 phase folded and binned on our new ephemeris. The upper two eclipse profiles are the *HIPPO 2010* and the *BVIT 2009* observations respectively. These correspond to the two newest data points in Fig. 2 which show a O-C shift of $\sim 30s$ with respect to each other on the quadratic subtracted O-C plot (upper plot Fig. 2). Therefore if the spot did indeed change locations, on the surface of the white dwarf, between these two observations then we should observe a corresponding relative phase shift between spot ingress/egress to that of the white dwarf photosphere ingress/egress. However one can see that the beginning of the white dwarf photosphere egress (solid vertical line at phase ~ 0.026) is consistently $\sim 40s$ (0.005 phase) ahead of the spot egress (vertical grey bars) between these two observations. Thus, one would have expected the relative time difference between the white dwarf photosphere and spot to be shorter by $\sim 30s$ between the two observations and not approximately equal as observed. Therefore we conclude that the spot has not moved on the surface of the white dwarf during these observations, at least within our measurable errors of about 1-5s. The same relative phase difference (spot, white dwarf photosphere) is also apparent in the other eclipse profiles in which the spot and white dwarf photosphere are resolved (see the next five plots in Fig. 1 corresponding to the *SALTICAM 2007*, *UCTPOL 2005*, *SWIFT 2002*, *UCTPOL 2002* and *SCAM 1999* observations). Furthermore, the same unchanging relative time differences are seen in the ingresses, although the white dwarf photosphere ingress emission may be complicated by an additional contribution from the accretion stream. The stream is not visible during the white dwarf photosphere egress, which can be understood from simple eclipse geometrical arguments, and confirmed through *HST* UV spectroscopy (Stockman & Schmidt 1996).

We note, however, that the longitude of the accretion spot should be expected to change during different accretion states. For example, Schwobe et al. (2001) calculated a change in spot longitude of $\sim 10^\circ$ between high and intermediate accretion states in the eclipsing polar HU Aqr. This would translate to about a shift of $\sim 2-3s$ in the O-C values (Schwarz et al. 2009) which therefore cannot account for the observed O-C values. This implies that if there was a similar spot motion in UZ For during different accretion states, it cannot account for the large shift seen in the measured O-C values.

Additionally there was not any measurable movement of the spot in latitude during our observations. This is apparent from table 1 where the eclipse width measurements agree within errors: a change in spot latitude would have resulted in a corresponding change in eclipse length.

5 SUMMARY AND CONCLUSION

We have detected departures in the eclipse times of UZ For from a simple quadratic ephemeris of up to $\sim 60s$. The departures are suggestive of two periodicities of ~ 16 and ~ 5.25 years. The two favoured mechanisms to drive the periodic-

ities are either two giant extrasolar planets as companions to the binary or a magnetic cycle mechanism (e.g. Applegate's mechanism) of the secondary star. However, Applegate's mechanism would require the entire radiant energy output of the secondary and therefore would seem to be the least likely of the two, barring any further refinements in the effect of magnetic fields (e.g. Lanza 1998). A two planet model is also problematic given the quality of the data in that a high eccentric orbit, for at least one of the planets, seems to be required to fully capture all of the eclipse times.

If it can be confirmed that the residuals are due to a third and a fourth body, then the planets either formed in a pre-common envelope circumbinary protoplanetary disc (first generation) or in a disc that resulted from the common envelope (CE) phase (second generation: Perets 2010). The separation of the progenitor binary is of the order of a few AU, comparable to that of the planets, which implies that only second generation planets could have formed at the orbits suggested here. However, Beuermann et al (2010a) suggested for the planets around NN Ser, a slowly expanding CE could provide the dynamical force to drag inwards planets formed further out, which would have otherwise been lost to the system due to the decrease in mass of the central binary (Alexander et al. 1976). In either case, we note that the semi-major axis of even the shortest period object poses no problem for orbit stability (Holman & Wiegert 1999).

It is intriguing that Qian et al (2011) propose a very similar two elliptical model fit for the polar HU Aqr, also using eclipse timing results. In particular they also find that the larger ellipse requires a high eccentricity (0.51) to correctly capture all of the data. Therefore, their two planet model for HU Aqr seems to have a similar problem with orbit instabilities that we have found for UZ For.

As yet there is insufficient data on UZ For to identify conclusively the mechanism responsible for the periodic changes in its eclipse times, and indeed more than one mechanism could be present. Further good signal/noise, high time resolved observations of UZ For and other similarly eclipsing systems are encouraged.

6 ACKNOWLEDGMENTS

We thank for referee for an insightful report that has significantly improved the paper.

This material is based upon work supported financially by the National Research Foundation. Any opinions, findings and conclusions or recommendations expressed in this material are those of the author(s) and therefore the NRF does not accept any liability in regard thereto.

Some of the observations reported in this paper were obtained with the Southern African Large Telescope (SALT).

Some of the data presented in this paper were obtained from the Multi-mission Archive at the Space Telescope Science Institute (MAST). STScI is operated by the Association of Universities for Research in Astronomy, Inc., under NASA contract NAS5-26555. Support for MAST for non-HST data is provided by the NASA Office of Space Science via grant NAG5-7584 and by other grants and contracts.

We would also like to thank Drs. Jean Dupuis, Phil Hodge and Damian J. Christian for their invaluable help when reducing EUVE and HST archival data.

REFERENCES

- Alexander M. E., Chau W. Y., & Henriksen R. N. 1976, *ApJ*, 204, 879
- Allen R. G., Berriman G., Smith P. S. & Schmidt G. D., 1989, 347, 426
- Applegate J. H., 1992, *ApJ*, 385, 621
- Bailey J. A. & Cropper M., 1991, *MNRAS*, 253, 27
- Brinkworth C. S., Marsh T. R., Dhillon V. S., & Knigge C., 2006, *MNRAS*, 365, 287
- Berriman G. & Smith P. S., 1988, *ApJ*, 329, L97
- Beuermann K. et al. 2010a, *A&A*, 521, L60
- Beuermann K. et al. 2010b, *A&A*, 526, A53
- Beuermann K., Thomas H.-C. & Schwöpe A. D., 1988, *A&A*, 195, L15
- de Bruijne J. H. J., Reynolds A. P., Perryman M. A. C., Favata F. & Peacock A., 2002, *SPIE*, *Optical Engineering* 41(06), 1158
- Campbell R. K., Harrison T. E., Mason E, Howell S. & Schwöpe A. D., 2008, *ApJ*, 678, 1304
- Crawford S. M., et al. 2010, *spie*, 7737, 54
- Cropper M. S., 1985, *MNRAS*, 212, 709
- Cropper M. S., 1990, *Space Sci. Rev.* 54, 195
- Dai Z. -B., Qian S.-B., Fernandez Lajus E. & Baume G. L., 2010, *arXiv:1007.4070v1*
- Eastman J., Siverd R. & Scott Gaudi B., 2010, *arXiv:1005.4415v2*
- Ferrario L., Wickramasinghe Dayal T., Bailey J. A., Tuohy I. R. & Hough J. H., 1989, *ApJ*, 337, 832
- Giommi P., Angelini L., Osborne J., Stella L., Tagliaferri G., Beuermann K., & Thomas H.-C., 1987, *IAU Circ. No.* 4486
- Holman M. J. & Wiegert P. A. 1999, *AJ*, 117, 621
- Imamura J. N. & Steiman-Cameron T. Y., 1998, *ApJ*, 501, 830
- Imamura J. N., Steiman-Cameron T. Y. & Wolff M. T., 2000, *PASP*, 112, 18
- Lanza A. F., Rodonó M., Rosner R., 1998, *MNRAS*, 296, 893
- Mason K. O., et al 2001, *A&A*, 365, L36
- O'Donoghue D., et al., 2006, *MNRAS*, 372, 151
- Osborne J.P., Giommi P., Angelini L., Tagliaferri G. & Stella L. 1988, *ApJ*, L45
- Parsons S. G. et al., 2010, *MNRAS*, 407, 2362
- Patterson J., 1984, *ApJS*, 54, 443
- Patterson J., 1994, *PASP*, 106, 209
- Perets H. B. 2010, *arXiv:1001.0581*
- Perryman M. A. C. et al. 2001, *MNRAS*, 324, 899
- Potter S. B. et al 2010, *MNRAS*, 402, 1161
- Qian S. -B., Liao W. -P., Zhu L.-Y. & Dai Z.-B. 2010, *ApJ*, 708, L66
- Qian S. -B. et al 2011, *MNRAS*, in press
- Ramsay G., 1994, *IBVS*, No. 4075
- Rappaport S., Verbunt F. & Joss P. C., 1983, *ApJ*, 275, 731
- Roming P. W. A., 2005, *SSRv*, 120, 95
- Ritter H., Kolb U., 2003, *A&A*, 404, 301 (update RKcat7.9)
- Schwarz R. et al. 2009, *A&A*, 496, 833
- Siegmund O. H. W., McPhate J., Tremsin A., Vallerga J. V., Welsh B. Y. & Wheatley J. M., 2008, *AIPC*, 984, 103
- Schwarz R., et al. 2009, *A&A*, 496, 833
- Schwöpe A. D., Schwarz R., Sirk M. & Howell S. B., 2001, *A&A*, 375, 419
- Schwöpe A. D., Hambaryan V., Schwarz R., Kanbach G. & Gänsicke B. T., 2002, *A&A*, 392, 541
- Stockman H. S. & Schmidt G. D., 1996, *ApJ*, 468, 883
- Warner B. 1995, *Cataclysmic Variable Stars*, Cambridge Astrophysics Series 28, Cambridge University Press
- Warren J. K., Sirk M. M. & Vallerga J. V., 1995, 445, 909